



## Article

# Synthesis and Luminescent Properties of Barium Molybdate Nanoparticles

Maria Gancheva <sup>1,\*</sup>, Reni Iordanova <sup>1</sup> , Iovka Koseva <sup>1</sup>, Georgi Avdeev <sup>2</sup> , Gergana Burdina <sup>1</sup> and Petar Ivanov <sup>3</sup>

<sup>1</sup> Institute of General and Inorganic Chemistry, Bulgarian Academy of Sciences, “Acad. G. Bonchev” Str., bl. 11, 1113 Sofia, Bulgaria; reni@svr.igic.bas.bg (R.I.); ikosseva@svr.igic.bas.bg (I.K.); g.naburdina@abv.bg (G.B.)

<sup>2</sup> Institute of Physical Chemistry “Acad. Rostislav Kaischew”, Bulgarian Academy of Sciences, “Acad. G. Bonchev” Str., bl. 11, 1113 Sofia, Bulgaria; g\_avdeev@ipc.bas.bg

<sup>3</sup> Institute of Optical Materials and Technologies “Acad. Jordan Malinowski”, Bulgarian Academy of Sciences, “Acad. G. Bonchev” Str., bl. 109, 1113 Sofia, Bulgaria; petar@iomt.bas.bg

\* Correspondence: m.gancheva@svr.igic.bas.bg; Tel.: +359-2-979-3588

**Abstract:** BaMoO<sub>4</sub> was obtained via facile mechanochemical synthesis at room temperature and a solid-state reaction. An evaluation of the phase composition and structural and optical properties of BaMoO<sub>4</sub> was conducted. The influence of different milling speeds on the preparation of BaMoO<sub>4</sub> was explored. A shorter reaction time for the phase formation of BaMoO<sub>4</sub> was achieved using a milling speed of 850 rpm. A milling speed of 500 rpm led to partial amorphization of the initial reagents and to prolongation of the synthesis time of up to 3 h of milling time. Solid-state synthesis was performed via heat treatment at 900 °C for 15 h. X-ray diffraction analysis (XRD), infrared (IR) and UV diffuse reflectance (UV-Vis) and photoluminescence (PL) spectroscopy were carried out to characterize the samples. Independently of the method of preparation, the obtained samples had tetragonal symmetry. The average crystallite sizes of all samples, calculated using Scherrer’s formula, were in the range of 240 to 1540 Å. IR spectroscopy showed that more distorted structural MoO<sub>4</sub> units were formed when the compound was synthesized via a solid-state reaction. The optical band gap energy of the obtained materials was found to decrease from 4.50 to 4.30 eV with increasing crystallite sizes. Green- and blue-light emissions were observed for BaMoO<sub>4</sub> phases under excitation wavelengths of 330 and 488 nm. It was established that the intensity of the PL peaks depends on two factors: the symmetry of MoO<sub>4</sub> units and the crystallite sizes.

**Keywords:** BaMoO<sub>4</sub>; high-energy ball milling; solid-state reaction; nanoparticles; infrared absorption bands; optical band gaps; blue and green photoluminescence; color coordinates



**Citation:** Gancheva, M.; Iordanova, R.; Koseva, I.; Avdeev, G.; Burdina, G.; Ivanov, P. Synthesis and Luminescent Properties of Barium Molybdate Nanoparticles. *Materials* **2023**, *16*, 7025. <https://doi.org/10.3390/ma16217025>

Academic Editors: Alexander N. Obraztsov and Antonio Polimeni

Received: 20 September 2023

Revised: 31 October 2023

Accepted: 1 November 2023

Published: 3 November 2023



**Copyright:** © 2023 by the authors. Licensee MDPI, Basel, Switzerland. This article is an open access article distributed under the terms and conditions of the Creative Commons Attribution (CC BY) license (<https://creativecommons.org/licenses/by/4.0/>).

## 1. Introduction

BaMoO<sub>4</sub> is a compound that belongs to transition-metal oxides with a scheelite-type structure. This phase is an important material and has useful applications in different scientific and technical areas as photocatalysts [1], anode materials for lithium ion batteries (LIB) and sodium ion batteries (SIB) [2], solid-state lasers [3], phosphors [4,5] and host matrices for doping with Re<sup>3+</sup> ions [5–7]. BaMoO<sub>4</sub> possesses good thermal and chemical stability. It is a semiconductor material with wide optical band gap and high luminescence at room temperature [1,3–9]. In the scheelite structure, Ba ions are coordinated with eight oxygen atoms, and Mo ions are connected to four oxygen atoms, forming MoO<sub>4</sub> groups [10]. The MoO<sub>4</sub> structural unit plays an important role in the electronic structural order and luminescence properties. J.C. Sczancoski et al. reported that the photoluminescence (PL) emission is adjudicated to the MoO<sub>4</sub><sup>2−</sup> complex, where cations like Ca<sup>2+</sup>, Sr<sup>2+</sup> and Ba<sup>2+</sup> acts as lattice-modifying agents, affecting the photoluminescence property directly [11]. There are data that provide evidence that BaMoO<sub>4</sub> exhibits green and/or blue emissions at room temperature depending on its morphology, defects, crystallite size, different excitation sources and method of preparation [3–26]. The attention of researchers is focused on fast

chemical or physical synthesis of BaMoO<sub>4</sub> under mild conditions and establishing the relationship between its structure, morphology and luminescence properties [10,20–25]. BaMoO<sub>4</sub> particles with shuttle-like microcrystals and an octahedral form exhibit blue emission at room temperature [15]. According to L. Ma et al., BaMoO<sub>4</sub> with various morphologies, such as ellipsoid-like, peanut-like, cube-like and flower-like, with sizes above 0.25 μm, exhibited the highest, high, middle and lowest photoluminescent emissions at 560 nm [19]. On the other hand, BaMoO<sub>4</sub> with nest-like and decahedron particles show strong green emission and weak red emission [16]. Micron-octahedron and micron-flower BaMoO<sub>4</sub> obtained via the sonochemical method exhibited a strong and broad green emission peak with a maximum at around 508 nm [17]. Y. Wang et al. investigated the influence of defects and Jahn–Teller distorted MoO<sub>4</sub> symmetry on the shape and position of the blue emission of BaMoO<sub>4</sub> [20]. The blue emission of BaMoO<sub>4</sub> powder or film was registered under excitation wavelengths of 250, 280, 350, 360 and 370 nm [9,14,23,25]. Photoluminescence in the green range was visible at the same wavelengths and at higher ones [16,17,21]. According to many authors, the appearance of blue or green emissions strongly depend on the types of defects that form during the experimental conditions and the morphology of the final products [4,12,13,20,22]. Several studies have reported that morphological control can be used to adjust the photoluminescence properties in the crystallite phases with the scheelite-type structure [15–17]. In the literature, there are data that show that the PL intensity and position of band emissions depend on the thermal treatment conditions of powders [24,25].

Different physicochemical routes have been applied for the preparation of BaWO<sub>4</sub>, such as solid-state reactions [5], hydrothermal synthesis [2,4,9,18], the aqueous mineralization process [15], coprecipitation [13,21], the sonochemical method [1,17], microwave-assisted synthesis [14,23], sol-gel [6], the complex polymerization method [3,24], laser-induced synthesis [25] and mechanochemical synthesis [27–30]. For example, the BaMoO<sub>4</sub> phase obtained through the ball milling of initial mixtures of BaCO<sub>3</sub> + MoO<sub>3</sub> and BaCO<sub>3</sub> + Na<sub>2</sub>MoO<sub>4</sub> can be used in the NIR pigment applications [27]. X.B. Chen et al. applied the high-temperature ball milling (HTBM) method for the preparation of BaMoO<sub>4</sub>:Eu<sup>3+</sup> red phosphors [28]. On the other hand, AMoO<sub>4</sub> (A = Ba, Sr) films were fabricated via a ball-rotation-assisted solid/solution reaction at room temperature [29]. R.C. Lima et al. [31] reported that additional milling led to an increase in the intensity of the emission spectra. Mechanochemical treatment has several advantages, such as shorter reaction time, cost-effectiveness, simplicity and reliability. The mechanochemical activation of solids leads to the appearance of fresh areas and active defects, which improves their catalytic, electrical and optical characteristics. The focus of our group is on the effects of different ball milling conditions for faster synthesis of a variety of inorganic compounds at ambient temperature [32–34]. This motivated us to use mechanochemical treatment for the preparation of BaMoO<sub>4</sub>. The obtained structural and luminescent properties will be compared with those of BaMoO<sub>4</sub> obtained via a solid-state reaction.

## 2. Materials and Methods

### 2.1. Direct Mechanochemical Synthesis

The reagents used in mechanochemical treatment are BaCO<sub>3</sub> (Merck, purity 99.9%) and MoO<sub>3</sub> (Merck, purity 99.9%). The stoichiometric ratio of the starting materials was 1:1 and corresponded to crystal-phase BaMoO<sub>4</sub>. High-energy ball milling of the initial mixture was carried out in a planetary ball mill (Fritsch, Premium line, Pulverisette No 7) with two different milling speeds: 500 and 850 rpm. The grinding ball was 2.5 mm in diameter and the ball-to-powder mass ratio was 10:1. Activation was performed in an air atmosphere. To minimize the temperature during milling, the process was carried out for periods of 15 min, with rest periods of 5 min [32–34]. The labels of the milled samples were as follows: BaMoO<sub>4</sub>-I using a milling speed of 500 rpm, BaMoO<sub>4</sub>-II using milling speed of 850 rpm.

## 2.2. Solid-State Reaction

The starting materials for the solid-state reaction were the same as those used for the mechanochemical activation, i.e., BaCO<sub>3</sub> (Merck, 99.99%, Rahway, NJ, USA) and MoO<sub>3</sub> (Merck, 99.99%). The stoichiometric proportions of both components were mixed and homogenized in an agate mortar at room temperature. Subsequently, the mixture was transferred to an alumina crucible and thermally treated at 900 °C for 15 h in an electrical furnace. The as-prepared sample was marked as BaMoO<sub>4</sub>-III.

## 2.3. Characterizations

Phase identification of BaMoO<sub>4</sub> was confirmed via X-ray powder diffraction analysis (XRD). The X-ray powder diffraction study was performed using a Bruker D8 Advance instrument (Bruker, Billerica, MA, USA) equipped with a copper tube (CuK $\alpha$ ) and a position-sensitive LynxEye detector. The crystallite size and cell parameters were calculated using HighScore plus 4.5 and ReX software (ReX v. 0.9.3 build ID 202308221535 (2023-08-22)). The crystallite size (D) was measured via diffraction line analysis using the Scherrer equation while taking into account the 2 $\theta$  (angular positions), Int (integral intensity value) and FWHM (full width at half-maximum). LaB<sub>6</sub> (NIST standard 660c-<https://tsapps.nist.gov/srmext/certificates/660c.pdf>) was used as a standard [35]. The cell parameters were obtained after refinement of the diffraction lines using the pseudo-Voigt profile function.

Infrared spectra were registered in the range 1200–400 cm<sup>-1</sup> on a Nicolet-320 FTIR spectrometer using the KBr pellet technique with a spectral resolution of 2 nm. The diffuse reflectance UV-Vis spectra were recorded using a Thermo Evolution 300 UV-Vis Spectrophotometer (Thermo Fisher Scientific, Waltham, MA, USA) equipped with a Praying Mantis device (Harrick Scientific, Pleasantville, NY, USA). For taking background measurements, we used Spectralon. The PL emission spectra were measured using a Horiba Fluorolog 3-22 TCS spectrophotometer (Horiba, Kyoto, Japan) equipped with a 450 W Xenon Lamp (Edinburgh Instruments, Livingston, UK) as the excitation source. This automated modular system has the highest sensitivity among those available on the market, allowing for the measurement of light emission for practically any type of sample. We used double-grating monochromators with emissions in the range of 200–950 nm; Ex. and Em. Bandpasses of 0–15 nm, continuously adjustable from a computer; wavelength accuracy of +/−0.5 nm; and scan speed of 150 nm/s. All spectra were measured at room temperature.

## 3. Results and Discussion

### 3.1. XRD Analysis

Comparisons of the structure, crystallite size and symmetry of the MoO<sub>4</sub> units and the optical properties of the samples produced via mechanochemical and solid-state methods were performed. The milling speed is an important parameter during mechanochemical activation, and it was studied. The effects of both milling speeds (500 and 850 rpm) on the reaction time and phase formation of BaMoO<sub>4</sub> were established via X-ray diffraction analysis (Figure 1A,B). The XRD patterns of the initial mixture before high-energy milling treatment show the principal peaks of orthorhombic MoO<sub>3</sub> (PDF-98-035-0609) and orthorhombic BaCO<sub>3</sub> (PDF-98-001-5196). A low milling speed at 500 rpm for 1h led to a decrease in intensity and broadening of the diffraction lines on the initial reagents. This is a result of a decrease in particle sizes, destruction of the long-range order and partial amorphization. In the same X-ray pattern, a new diffraction line at 26.35°, typical for tetragonal BaMoO<sub>4</sub> (PDF-01-089-4570), was observed. Increasing the milling time up to 3 h caused the appearance of additional reflections characteristic of BaMoO<sub>4</sub>. The small intensity peak at 13.00° and amorphous halo indicate that the full reaction did not occur. The complete reaction between the activated reagents was finished after 5 h of milling time (Figure 1A). In order to verify the reaction time and phase formation of BaMoO<sub>4</sub>, we used a milling speed of 850 rpm. The higher milling speed led to the appearance of the principal peaks of BaMoO<sub>4</sub> after a shorter time of activation (15 min). But diffraction lines typical of unreacted MoO<sub>3</sub> were observed at 2 $\theta$  = 24° (Figure 1B). A single phase of tetragonal BaMoO<sub>4</sub> was synthesized

after 30 min of milling time, which is shorter compared to the reaction time activation was applied at 500 rpm. The phase formation of  $\text{BaMoO}_4$  at the higher milling speed is due to more effective solid-state diffusion between reagents during the ball–material collisions. Previously, we pointed out that  $\text{BaMoO}_4$  was obtained via different methods of preparation, which involved additives, solvents and prolonged heat treatment [4,9,13–18]. The obtained results demonstrated that activation via high-energy ball milling offers enough energy to generate a chemical reaction at room temperature. It was noted that the ball milling of the mixture of  $\text{BaCO}_3$  and  $\text{MoO}_3$  using the milling speed of 850 rpm produces tetragonal  $\text{BaMoO}_4$  with a faster reaction time. These results demonstrate that mechanochemical treatment is a more substantial approach to the rapid preparation of powder materials. Figure 1C exhibits the XRD pattern of  $\text{BaMoO}_4$  after heat treatment at  $900\text{ }^\circ\text{C}$  for 15 h. Remarkable narrowing of the diffraction lines was observed, which occurred due to the high crystallinity of  $\text{BaMoO}_4$  compared to the mechanochemically synthesized  $\text{BaMoO}_4$  powders. No additional diffraction lines were found, indicating that the obtained samples were a pure single phase when using both preparation techniques.

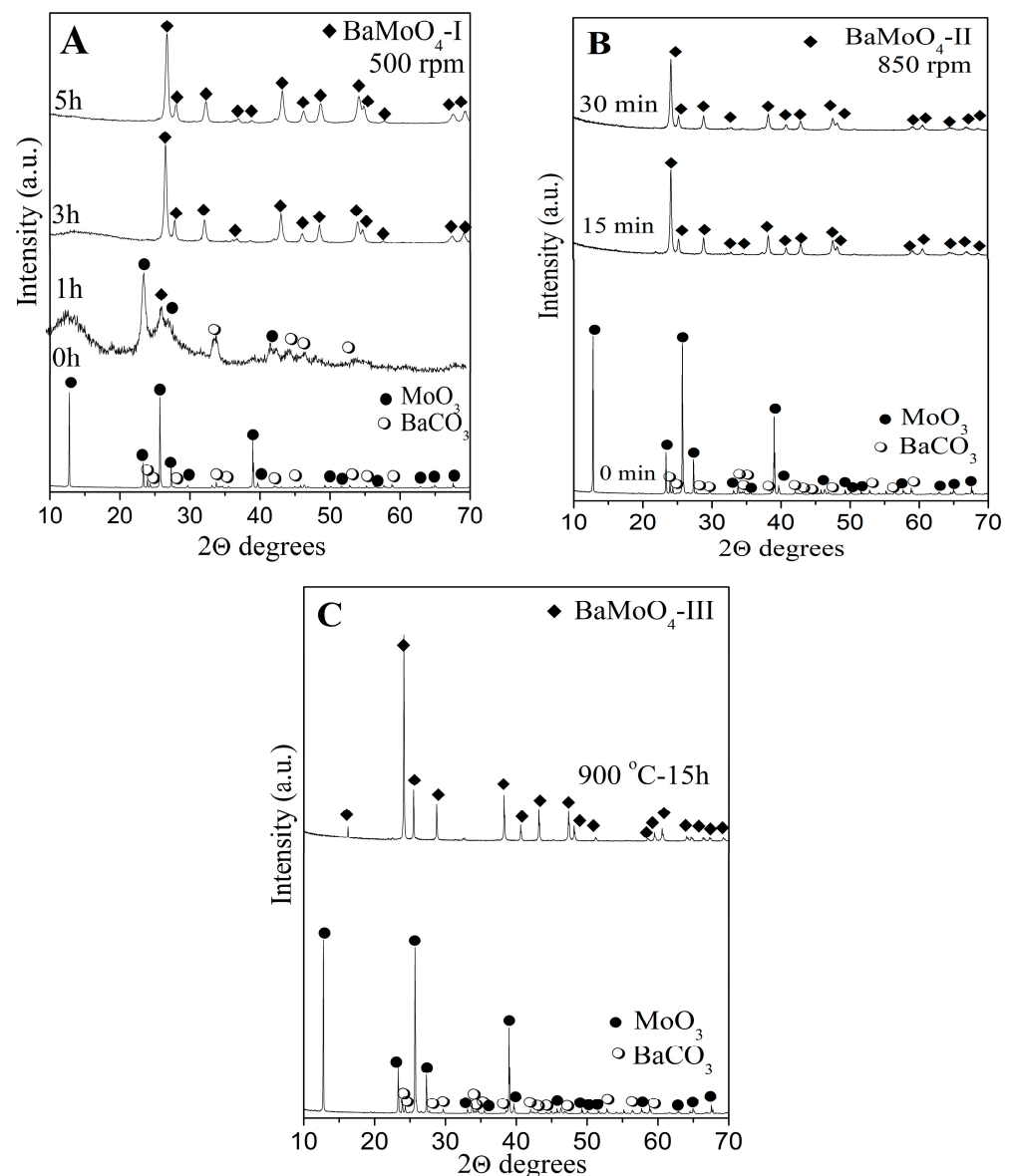


**Figure 1.** XRD patterns of the initial mixture and mechanochemically activated mixture at 500 rpm (A), mechanochemically activated mixture at 850 rpm (B) and  $\text{BaMoO}_4$  obtained after solid-state reaction (C).

Table 1 presents lattice parameters  $a$  and  $c$ , the volume of the unit cells and the average crystallite sizes for the  $\text{BaMoO}_4$  obtained via different methods of synthesis. A higher milling speed for a short time led to a slight increase in lattice parameters  $a$  and  $c$ , the volume of the unit cells and the average crystal size. This fact can be attributed to the increase in lattice defects due to higher energy caused by a higher milling speed. A rapid mechanochemical reaction induced a smaller crystallite size due to fast crystallite formation. In solid-state synthesis, the total number of defects significantly decreased, which is demonstrated by an increase in the crystallite size up to 1540 Å. Lattice parameter  $c$  decreased compared with those of  $\text{BaMoO}_4$ -I and  $\text{BaMoO}_4$ -II obtained after a shorter time of synthesis. This can be attributed to the clustering of point defects in the  $a$  plane, which was also indirectly confirmed via infrared analysis.

**Table 1.** Lattice parameter values, unit cell volumes and average crystallite sizes of  $\text{BaMoO}_4$  prepared using both methods.

Samples	$a = b$ (Å)	$c$ (Å)	Unit Cell Volume (Å <sup>3</sup> )	Average Crystallite Size (Å)
BaMoO <sub>4</sub> -I 5 h/500 rpm	5.5718 (9)	12.800 (3)	397.3864	240 (5)
BaMoO <sub>4</sub> -II 30 min/850 rpm	5.5811 (4)	12.819 (1)	399.2755	270 (5)
BaMoO <sub>4</sub> -III 900 °C-15 h	5.6083 (2)	12.7019 (5)	399.5213	1540 (4)
PDF-BaMoO <sub>4</sub>	5.58	12.82	399.17	-

### 3.2. Infrared Analysis

The phase formation of  $\text{BaMoO}_4$  using different methods of synthesis was confirmed via IR spectroscopy (Figure 2). On the other hand, this analysis is suitable to investigate the local structure of metal ions in the crystallite phases. The infrared spectra display one absorption band in the range of 820 to 835  $\text{cm}^{-1}$  due to the  $\nu_3$  vibration of the  $\text{MoO}_4$  structural units forming the crystalline structure of  $\text{BaMoO}_4$  [1,6,18,24]. The IR spectra of all  $\text{BaMoO}_4$  samples are similar. Small differences in the frequency of the main absorption mode were detected. The band position at 825 is shifted up to 835  $\text{cm}^{-1}$  and becomes more symmetric using the higher milling speed of 850 rpm. This fact can be attributed to the formation of more symmetric  $\text{MoO}_4$  units. The partial amorphization and longer milling time at the speed of 500 rpm favors the formation of a distorted  $\text{MoO}_4$  entity. The IR spectrum of  $\text{BaMoO}_4$  prepared via the solid-state reaction exhibits a more narrow and intense absorption band (820  $\text{cm}^{-1}$ ), an indication of the higher crystallinity of sample, which is confirmed via XRD analysis (Figure 1C and Table 1). In this case, the appearance of a shoulder at 860  $\text{cm}^{-1}$  is attributed to elimination of the  $\nu_3$  vibration degeneracy of  $\text{MoO}_4$  tetrahedra with different local symmetry [36]. This result can be attributed to the formation of more distorted Mo-tetrahedral groups due to the long sintering time. We can conclude that the mechanochemical activation at higher milling speed leads to the formation of more symmetrical  $\text{MoO}_4$  structural units. Bearing in mind the IR features, we expect that the obtained  $\text{BaMoO}_4$  powders will possess different luminescence behavior according to J.C. Sczancoski et al. [11].

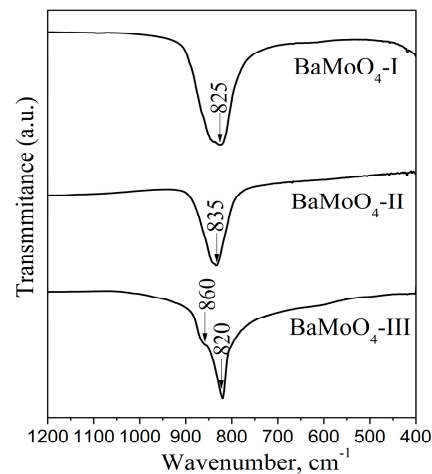


**Figure 2.** Infrared spectra of BaMoO<sub>4</sub> synthesized using different methods of preparation.

### 3.3. Ultraviolet–Visible Spectroscopy

Regarding the effects of the band gaps of inorganic materials on their luminescent and electrical properties, according to the literature data, the value of the optical band gap will increase with a decrease in crystallite size [12,37,38]. The UV-vis absorbance spectra of the obtained BaMoO<sub>4</sub> are shown in Figure 3. All samples exhibit one absorption peak in range 215–235 nm, which is attributed to the charge-transfer transitions within the MoO<sub>4</sub><sup>2−</sup> complex [1,3–8]. The observed UV-Vis spectra of our samples are closer to those of BaMoO<sub>4</sub> obtained via the hydrothermal method, the molten salt synthesis and the sonochemical route [4,8,17]. A slight shift in this peak is observed upon applying the different methods of preparation (Figure 3A). In the UV-Vis absorption spectrum of BaMoO<sub>4</sub>-III prepared via the solid-state reaction, a band at 300 nm is also observed. Bearing in mind the reported data, this band corresponds to the creation of the excitonic state in A<sup>2+</sup> ions (A<sup>2+</sup> = Ba, Sr, Ca) [3,39]. The optical band gap energy (E<sub>g</sub>) of the samples prepared via mechanochemical and solid-state methods was calculated using the Tauc equation [40].

$$\alpha h\nu = A (h\nu - E_g)^n,$$

where  $h$  is Planck's constant,  $\alpha$  is the absorption coefficient,  $\nu$  is the photon frequency,  $A$  is a constant,  $E_g$  is the optical band gap and  $n = 1/2$  is used for BaMoO<sub>4</sub>. Based on this equation, the band gaps of the investigated crystal phases are estimated to be above 4.30 eV, as illustrated in Figure 3B. The examined optical band gaps with respect to milling speed and time show a tendency to decrease in value with increasing the crystallite size (BaMoO<sub>4</sub>-I with  $D = 240 \text{ \AA}$  and  $E_g = 4.50 \text{ eV}$ ; BaMoO<sub>4</sub>-II with  $D = 270 \text{ \AA}$  and  $E_g = 4.47 \text{ eV}$ ). This tendency was also observed for BaMoO<sub>4</sub>-III ( $E_g = 4.30 \text{ eV}$  with  $D = 1540 \text{ \AA}$ ) prepared via the solid-state reaction. The smaller optical band gap suggests that the crystal structure of BaMoO<sub>4</sub>-III has more defects, which is established via X-ray analysis and IR spectroscopy. The formation of defects led to the induction of additional electronic states between the valence band and conduction band in the materials, resulting in a reduction in the  $E_g$  value. The values of the calculated band gaps for milled samples subjected to different speeds are slightly higher than those of samples synthesized via heat treatment at 900 °C. The obtained values of the optical band gaps are higher than those of BaMoO<sub>4</sub> obtained via hydrothermal synthesis, the coprecipitation method, laser-induced synthesis and the microwave plasma method [4,19,24,41]. According to W. Wang et al., materials with lower crystallite size and with larger values of the optical band gap ( $E_g$ ) possess higher luminescence intensity [37]. To better understand the correlation between the optical properties and crystal structure, we measured the PL spectra of the obtained BaMoO<sub>4</sub> samples.

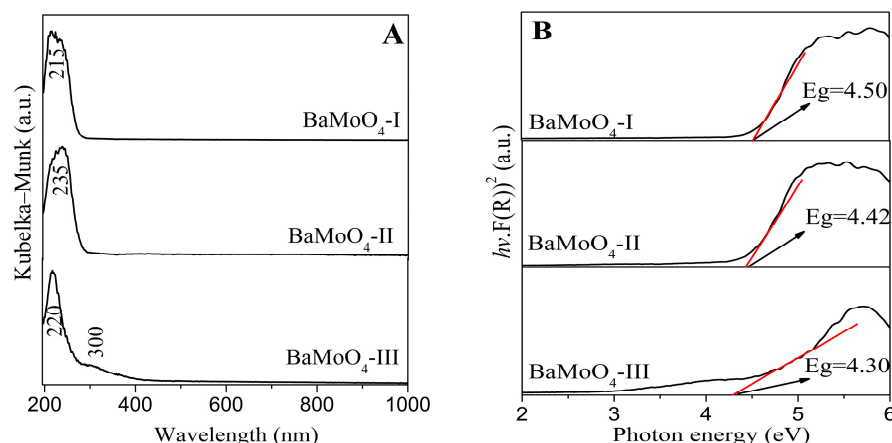


**Figure 3.** (A) UV-Vis spectra of BaMoO<sub>4</sub> obtained using different methods of synthesis; (B) Tauc's plot of BaMoO<sub>4</sub> obtained using different methods of synthesis.

### 3.4. Photoluminescence (PL) Analysis

The photoluminescence emission behavior of the three BaMoO<sub>4</sub> powders were investigated at room temperature and are presented in Figure 4. An asymmetric and intense blue peak with a maximum at 400 nm was recorded under excitation at 330 nm (Figure 4A). The profile of blue emission lines is similar to those of BaMoO<sub>4</sub> obtained via the hydrothermal and microwave-induced plasma methods [1,3]. The effect of ball milling speed/time on light emission was investigated and is discussed below. Significant differences were found for the investigated samples. The position of the maximum was changed from 400 to 405 nm for BaMoO<sub>4</sub>-I obtained using the milling speed of 500 rpm. The PL in the blue region was broader after longer milling time at the same rotation speed (BaMoO<sub>4</sub>-I). The lowest intensity was observed for BaMoO<sub>4</sub>-III obtained via the traditional solid-state reaction. A broad green symmetric emission centered at about 560 nm was observed under excitation at 488 nm (Figure 4B). The shape of the PL line is typical of inorganic metal oxide with a scheelite-type structure [20,42]. The PL strength in the green region is almost the same for both samples obtained via mechanochemical activation using milling speeds of 500 and 850 rpm, respectively (Figure 4B). In this case, the broadest peak and lowest intensity were observed for BaMoO<sub>4</sub>-III obtained via the solid-state route. S. Raghunath et al. reported that BaMoO<sub>4</sub> obtained via the precipitation method possesses lower emission intensity in the range of 510 to 590 nm [43]. According to the literature data, blue emission is attributed to charge-transfer transitions within the [MoO<sub>4</sub>] complex, while the green emission is due to intrinsic distortion in the [MoO<sub>4</sub>] tetrahedron group and can arise due to various factors, like crystallinity, morphology, surface defects, etc. [3,16,20,21,44]. In this instance, the variation in the PL intensity of our samples was caused by the different preparation methods, crystallite sizes and main structural units, i.e., MoO<sub>4</sub>. The above results show that BaMoO<sub>4</sub>-I prepared after a brief milling period using a milling speed of 850 rpm exhibited higher blue luminescence intensity than samples obtained at a lower milling speed of 500 rpm and solid-state reaction, respectively. The broader peak and lower intensity in the blue and green emissions of BaMoO<sub>4</sub>-III prepared via the solid-state reaction are probably due to the presence of more distorted MoO<sub>4</sub> units according to the obtained IR results. This result is in good agreement with those reported by R. Künzel et al. [4]. The photoluminescence results indicated that the BaMoO<sub>4</sub> prepared via mechanochemical activation had a small number of defects. The other factor that affected the PL intensity was the crystallite size, which was clearly observed in both emissions. Our investigations show that the BaMoO<sub>4</sub>-I and BaMoO<sub>4</sub>-II obtained via direct mechanochemical synthesis with lower crystallite sizes (240 and 270 Å) possess higher luminescence strength. Similar results have been reported by other authors [37,45]. On the other hand, the lower values of the optical band gap (E<sub>g</sub>) and PL emissions of BaMoO<sub>4</sub> produced via solid-state synthesis were impacted by the formation of distorted MoO<sub>4</sub> and higher crystallite sizes. From the

obtained PL data, we can conclude that symmetric  $\text{MoO}_4$  units and lower crystallite size are important factors for improving luminescence efficiency. Our future investigations will be focused on the mechanochemical synthesis  $\text{BaMoO}_4$  doped with different rare-earth ions ( $\text{Eu}^{3+}$ ,  $\text{Dy}^{3+}$  and  $\text{Tb}^{3+}$ ) for obtaining materials with multiple colors. As  $\text{BaMoO}_4$  matrix luminescence is blue or green, the first step will be the preparation of  $\text{Dy}^{3+}$ -doped  $\text{BaMoO}_4$  to achieve the white light emission.

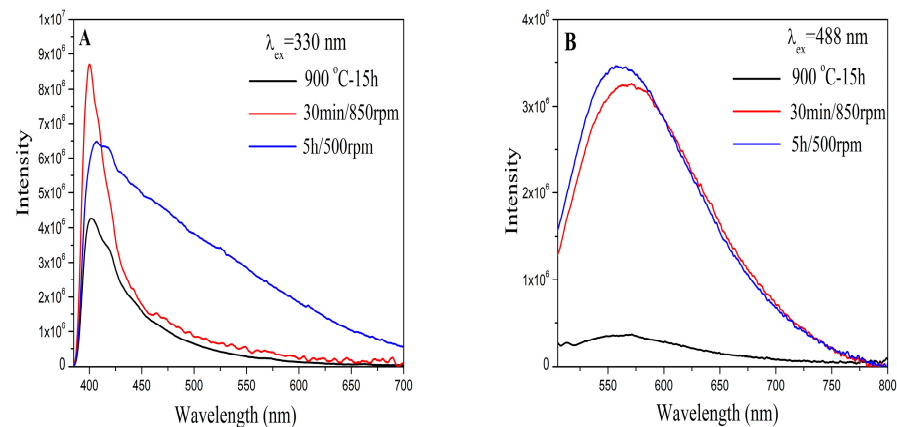


**Figure 4.** Photoluminescence emission spectra of  $\text{BaMoO}_4$  obtained using different methods of synthesis under excitation at 330 nm (A) and 488 nm (B).

Color chromaticity coordinates are another feature that impacts optical properties. The values of the  $x$  and  $y$  coordinates of  $\text{BaMoO}_4$  powders were calculated using a standard procedure from their emission spectra and are presented in Figure 5A,B. It can be seen from the figures that they fall within the blue and green areas, respectively. The values of the CIE parameters of the obtained  $\text{BaMoO}_4$  samples are summarized in Table 2.

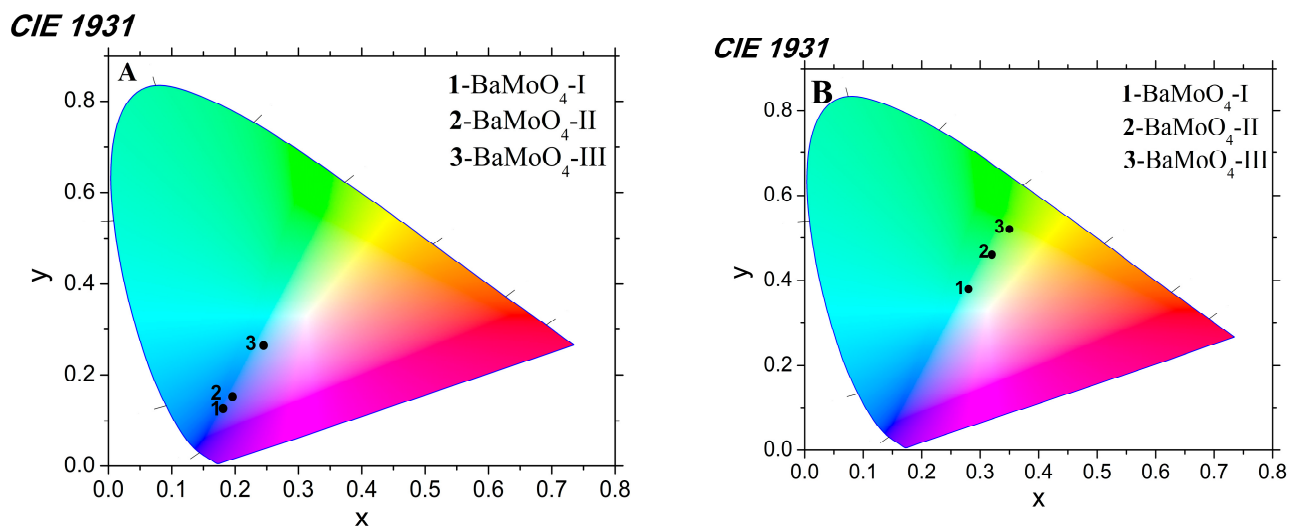


**Figure 5.** CIE color coordinates of obtained  $\text{BaMoO}_4$  samples under excitation at 330 (A) and 488 nm (B).

**Table 2.** CIE color coordinates of obtained  $\text{BaMoO}_4$  samples under excitation at 330 and 488 nm.

Samples	$x, y$ (exc. 330 nm)	$x, y$ (exc. 488 nm)
$\text{BaMoO}_4$ -I	0.18, 0.12	0.28, 0.38
$\text{BaMoO}_4$ -II	0.20, 0.15	0.32, 0.46
$\text{BaMoO}_4$ -III	0.25, 0.26	0.35, 0.52



#### 4. Conclusions

In this work we investigate the correlation between the method of synthesis and the structural and optical properties of BaMoO<sub>4</sub>. Nanoparticles of the BaMoO<sub>4</sub> with a scheelite-type structure were prepared via a mechanochemical approach and a solid-state reaction. It was established that the milling speed is a crucial parameter for the rapid synthesis of BaMoO<sub>4</sub> at room temperature. The crystallite size of both materials obtained at different speeds of mechanochemical activation (500 and 850 rpm) were in the nanoscale range, up to 300 Å. The calculated optical band gaps were wider (above 4.47 eV). The deformation of the structural units that formed the BaMoO<sub>4</sub> compound was established via IR spectroscopy. It was found that the optical properties depend on the applied method of synthesis, and therefore, on the structural entity distortion and the crystallite size. Mechanochemically prepared BaMoO<sub>4</sub> had stronger and more symmetric photoluminescence spectra in the blue and green regions compared to the sample prepared via solid-state synthesis. The symmetry of MoO<sub>4</sub> structural units and crystallite size are both factors that affected the emission intensity. The obtained results suggest the potential use of BaMoO<sub>4</sub> in the production of optoelectronic devices.

**Author Contributions:** Conceptualization, M.G., I.K. and R.I.; methodology, M.G.; software, G.A. and XRD; investigation, G.B.; writing—original draft preparation, M.G., writing—review and editing, I.K. and R.I.; PL measurements and visualization, P.I. All authors have read and agreed to the published version of the manuscript.

**Funding:** The authors acknowledge the project Д01-272-“European Network on Materials for Clean Technologies” for providing the opportunity to present the results at the SizeMat4 conference as well as for the financial publication support.

**Institutional Review Board Statement:** Not applicable.

**Informed Consent Statement:** Not applicable.

**Data Availability Statement:** Not applicable.

**Acknowledgments:** The authors acknowledge the project Д01-272-“European Network on Materials for Clean Technologies” for providing the opportunity to present the results at the SizeMat4 conference as well as for the financial publication support. Research equipment from the Distributed Research Infrastructure INFRAMAT, part of Bulgarian National Roadmap for Research Infrastructures, supported by the Bulgarian Ministry of Education and Science, was used in this investigation.

**Conflicts of Interest:** The authors declare no conflict of interest.

#### References

1. Bazarganipou, M. Synthesis and characterization of BaMoO<sub>4</sub> nanostructures prepared via a simple sonochemical method and their degradation ability of methylene blue. *Ceram. Int.* **2016**, *42*, 12617–12622. [[CrossRef](#)]
2. Ma, X.; Zhao, W.; Wu, J.; Jia, X. Preparation of flower-like BaMoO<sub>4</sub> and application in rechargeable lithium and sodium ion batteries. *Mater. Lett.* **2017**, *188*, 248–251. [[CrossRef](#)]
3. Marquesa, A.P.A.J.; Melo, D.M.A.; Longo, E.; Paskocimasa, C.A.; Pizanic, P.S.; Leite, E.R. Photoluminescence properties of BaMoO<sub>4</sub> amorphous thin films. *J. Solid State Chem.* **2005**, *178*, 2346–2353. [[CrossRef](#)]
4. Künzel, R.; Latini, R.M.; Umisedo, N.K.; Yoshimura, E.M.; Okuno, E.; Courrol, L.C.; Marques, A.P.A. Effects of beta particles irradiation and thermal treatment on the traps levels structure and luminescent properties of BaMoO<sub>4</sub> phosphor. *Ceram. Int.* **2019**, *45*, 7811–7820. [[CrossRef](#)]
5. Wu, B.; Yang, W.; Liu, H.; Huang, L.; Zhao, B.; Wang, C.; Xu, G.; Lin, Y. Fluorescence spectra and crystal field analysis of BaMoO<sub>4</sub>:Eu<sup>3+</sup> phosphors for white light-emitting diodes. *Spectrochim. Acta A Mol. Biomol. Spectrosc.* **2014**, *123*, 12–17. [[CrossRef](#)]
6. Jena, P.; Gupta, S.K.; Natarajan, V.; Sahu, M.; Satyanarayana, N.; Venkateswarlu, M. Structural characterization and photoluminescence properties of sol-gel derived nanocrystalline BaMoO<sub>4</sub>:Dy<sup>3+</sup>. *J. Lum.* **2015**, *158*, 203–210. [[CrossRef](#)]
7. Sharath, R.A.; Rahulan, K.M.; Flower, N.A.L.; Sujatha, R.A.; Vinitha, G.; Rejeev, L.R.; Saha, T.; Prakashbabu, D. Third-order nonlinear optical characteristics of Er<sup>3+</sup>-doped BaMoO<sub>4</sub> nanostructures. *J. Mater. Sci. Mater. Electron.* **2022**, *33*, 8542–8550. [[CrossRef](#)]
8. Afanasiev, P. Molten salt synthesis of Barium molybdate and tungstate microcrystals. *Mater. Lett.* **2017**, *61*, 4622–4626. [[CrossRef](#)]

9. Alencar, L.D.S.; Mesquita, A.; Feitosa, C.A.C.; Balzer, R.; Probst, L.F.D.; Marcelo, D.C.B.; Rosmaninho, G.; Fajardo, H.V.; Bernardi, M.I.B. Preparation, characterization and catalytic application of Barium molybdate ( $\text{BaMoO}_4$ ) and Barium tungstate ( $\text{BaWO}_4$ ) in the gas-phase oxidation of toluene. *Ceram. Int.* **2017**, *43*, 4462–4469. [CrossRef]
10. Oliveira, M.C.; Gracia, L.; Nogueira, I.C.; Gurgel, M.F.C.; Mercury, J.M.R.; Longo, E.; Andres, J. On the morphology of  $\text{BaMoO}_4$  crystals: A theoretical and experimental approach. *Cryst. Res. Technol.* **2016**, *51*, 634–644. [CrossRef]
11. Sczancoski, J.C.; Bomio, M.D.R.; Cavalcante, L.S.; Joya, M.R.; Pizani, P.S.; Varela, J.A.; Longo, E.; Siu, L.M.; Andres, J.A. Morphology and Blue Photoluminescence Emission of  $\text{PbMoO}_4$  Processed in Conventional Hydrothermal. *J. Phys. Chem.* **2009**, *C113*, 5812–5822. [CrossRef]
12. Marques, A.P.A.; Picon, F.C.; Melo, D.M.A.; Pizani, P.S.; Leite, E.R.; Varela, J.A.; Longo, E. Effect of the order and disorder of  $\text{BaMoO}_4$  powders in photoluminescent properties. *J. Fluoresc.* **2008**, *18*, 51–59. [CrossRef] [PubMed]
13. Phuruangat, A.; Thongtem, T.; Thongtem, S. Precipitate synthesis of  $\text{BaMoO}_4$  and  $\text{BaWO}_4$  nanoparticles at room temperature and their photoluminescence properties. *Superlattices Microstruct.* **2012**, *52*, 78–83. [CrossRef]
14. Lim, C.S. Microwave-assisted synthesis and photoluminescence of  $\text{MMoO}_4$  (M Ca, Ba) particles via a metathetic reaction. *J. Lum.* **2012**, *132*, 1774–1780. [CrossRef]
15. Wu, X.; Du, J.; Li, H.; Zhang, M.; Xi, B.; Fan, H.; Zhu, Y.; Qian, Y. Aqueous mineralization process to synthesize uniform shuttle-like  $\text{BaMoO}_4$  microcrystals at room temperature. *J. Solid State Chem.* **2017**, *180*, 3288–3295. [CrossRef]
16. Luo, Z.; Li, H.; Shu, H.; Wang, K.; Xia, J.; Yan, Y. Synthesis of  $\text{BaMoO}_4$  nestlike nanostructures under a new growth mechanism. *Cryst Growth Des.* **2008**, *8*, 2275–2281. [CrossRef]
17. Zhang, J.; Li, L.; Zi, W.; Zou, L.; Gana, S.; Ji, G. Size-tailored synthesis and luminescent properties of three-dimensional  $\text{BaMoO}_4$ ,  $\text{BaMoO}_4\cdot\text{Eu}^{3+}$  micron-octahedrons and micron-flowers via sonochemical route. *Luminescence* **2015**, *30*, 280–289. [CrossRef]
18. Luo, Y.S.; Zhang, W.D.; Dai, X.J.; Yang, Y.; Fu, S.Y. Facile Synthesis and luminescent properties of novel flowerlike  $\text{BaMoO}_4$  nanostructures by a simple hydrothermal route. *J. Phys. Chem. C* **2009**, *113*, 4856–4861. [CrossRef]
19. Ma, L.; Sun, Y.; Gao, P.; Yin, Y.; Qin, Z.; Zhou, B. Controlled synthesis and photoluminescence properties of hierarchical  $\text{BaXO}_4$  (X = Mo, W) nanostructures at room temperature. *Mater. Lett.* **2010**, *64*, 1235–1237. [CrossRef]
20. Wang, Y.; Gao, H.; Wang, S.; Fang, L.; Chen, X.; Yu, C.; Tang, S.; Liu, H.; Yi, Z.; Yang, H. Facile synthesis of  $\text{BaMoO}_4$  and  $\text{BaMoO}_4/\text{BaWO}_4$  heterostructures with type -I band arrangement and enhanced photoluminescence properties. *Adv. Powder Technol.* **2021**, *32*, 4186–4197. [CrossRef]
21. Cavalcante, L.S.; Sczancoski, J.C.; Tranquilin, R.L.; Joya, M.R.; Pizani, P.S.; Varela, J.A.; Longo, E.  $\text{BaMoO}_4$  powders processed in domestic microwave-hydrothermal: Synthesis, characterization and photoluminescence at room temperature. *J. Phys. Chem. Solids* **2008**, *69*, 2674–2680. [CrossRef]
22. Sczancoski, J.C.; Cavalcante, L.S.; Marana, N.L.; Silva, R.O.; Tranquilin, R.L.; Joya, M.R.; Pizani, P.S.; Varela, J.A.; Sambrano, J.R.; Li, M.S.; et al. Electronic structure and optical properties of  $\text{BaMoO}_4$  powders. *Curr. Appl. Phys.* **2010**, *10*, 614–624. [CrossRef]
23. Ryu, J.H.; Yoon, J.W.; Lim, C.S.; Shim, K.B. Microwave-assisted synthesis of barium molybdate by a citrate complex method and oriented aggregation. *Mater. Res. Bull.* **2005**, *40*, 1468–1476. [CrossRef]
24. Marques, A.P.A.; Melo, D.M.A.; Longo, E.; Paskocimas, C.A.; Pizani, P.S.; Leite, E.R. Photoluminescent  $\text{BaMoO}_4$  nanopowders prepared by complex polymerization method (CPM). *J. Solid State Chem.* **2006**, *179*, 671–678. [CrossRef]
25. Ryu, J.H.; Kim, K.M.; Mhim, S.W.; Park, G.S.; Eun, J.W.; Shim, K.B.; Lim, C.S. Laser-induced synthesis of  $\text{BaMoO}_4$  nanocolloidal suspension and its optical properties. *Appl. Phys.* **2008**, *A92*, 407–412. [CrossRef]
26. Pereira, W.S.; Sczancoski, J.C.; Lango, E. Tailoring the photoluminescence of  $\text{BaMoO}_4$  and  $\text{BaMoO}_4$  hierarchical architectures via precipitation induced by a fast precursor injection. *Mater. Lett.* **2021**, *293*, 129681. [CrossRef]
27. Baby, O.M.; Balamurugan, S.; Ashika, S.A.; Fathima, T.K.S. Synthesis and characterization of high NIR reflecting ecofriendly  $\text{BaMoO}_4$  pigments in scheelite family. *Emergent Mater.* **2022**, *5*, 1213–1225. [CrossRef]
28. Chen, X.B.; Shao, Z.B.; Tian, Y.W. New method for preparation of luminescent lanthanide materials  $\text{BaMoO}_4\cdot\text{Eu}^{3+}$ . *Mater. Technol.* **2011**, *26*, 67–70. [CrossRef]
29. Rangappa, D.; Fujiwara, T.; Watanabe, T.; Yoshimura, M. Fabrication of  $\text{AMoO}_4$  (A = Ba, Sr) film on Mo substrate by solution reaction assisted ball-rotation. *Mater. Res. Bull.* **2008**, *43*, 3155–3163. [CrossRef]
30. Xiao, E.C.; Li, J.; Wang, J.; Xing, C.; Guo, M.; Qiao, H.; Wang, Q.; Qi, Z.M.; Dou, G.; Shi, F. Phonon characteristics and dielectric properties of  $\text{BaMoO}_4$  ceramic. *J. Mater.* **2018**, *4*, 383–389. [CrossRef]
31. Lima, R.C.; Anicete-Santos, M.; Orhan, E.; Maurera, M.A.M.A.; Souza, A.G.; Pizani, P.S.; Leite, E.R.; Varela, J.A.; Lango, E. Photoluminescent property of mechanically milled  $\text{BaWO}_4$  powder. *J. Lim.* **2007**, *126*, 741–746. [CrossRef]
32. Dimitriev, Y.; Gancheva, M.; Iordanova, R. Effects of the mechanical activation of zinc carbonate hydroxide on the formation and properties of zinc oxides. *J. Alloys Compd.* **2012**, *519*, 161–166. [CrossRef]
33. Gancheva, M.; Szafraniak-Wiza, I.; Iordanova, R.; Piroeva, I. Comparative analysis of nanocrystalline  $\text{CuWO}_4$  obtained by high-energy ball milling. *J. Chem. Techn. Metall.* **2019**, *54*, 1233–1239. Available online: [https://journal.uctm.edu/node/j2019-6/14\\_18-220\\_p\\_1233-1239.pdf](https://journal.uctm.edu/node/j2019-6/14_18-220_p_1233-1239.pdf) (accessed on 18 September 2023).
34. Gancheva, M.; Iordanova, R.; Mihailov, L. Direct mechanochemical synthesis and characterization of  $\text{SrWO}_4$  nanoparticle. *Bulg. Chem. Commun.* **2022**, *54*, 337–342. Available online: [http://bcc.bas.bg/BCC\\_Volumes/Volume\\_54\\_Number\\_4\\_2022/bcc-54-4-2022-337-342-gancheva-nc02.pdf](http://bcc.bas.bg/BCC_Volumes/Volume_54_Number_4_2022/bcc-54-4-2022-337-342-gancheva-nc02.pdf) (accessed on 18 September 2023).

35. Black, D.; Mendenhall, M.; Henins, A.; Filliben, J.; Cline, J. The Certification of Standard Reference Material 660C for Powder Diffraction, Powder Diffraction. 2020. Available online: <https://tsapps.nist.gov/srmext/certificates/660c.pdf> (accessed on 2 November 2023).
36. Iordanova, R.S.; Milanova, M.K.; Kostov, K.L. Glass formation in the MoO<sub>3</sub>–CuO system. *Phys. Chem. Glas. Eur. J. Glass Sci. Technol. B.* **2006**, *47*, 631–637. Available online: <https://www.ingentaconnect.com/content/sgt/ejgst/2006/00000047/00000006/art00003> (accessed on 18 September 2023).
37. Wang, W.; Pan, Y.; Zhang, W.; Liu, X.; Li, L. The size effect to O<sup>2-</sup>—Ce<sup>4+</sup> charge transfer emission and band gap structure of Sr<sub>2</sub>CeO<sub>4</sub>. *Luminescence* **2018**, *33*, 907–912. [[CrossRef](#)]
38. Bandi, S.; Vidyasagar, D.; Adil, S.; Singhd, M.K.; Basud, J.; Srivastav, A.K. Crystallite size induced bandgap tuning in WO<sub>3</sub> derived from nanocrystalline tungsten. *Scr. Mater.* **2020**, *176*, 47–52. [[CrossRef](#)]
39. Spassky, D.A.; Ivanov, S.N.; Kolobanov, V.N.; Mikhailin, V.V.; Zemskov, V.N.; Zadneprovski, B.I.; Potkin, L.I. Optical and luminescent properties of the lead and barium molybdates. *Radiat. Meas.* **2004**, *38*, 607–610. [[CrossRef](#)]
40. Tauc, J. Absorption edge and internal electric fields in amorphous semiconductors. *Mater. Res. Bull.* **1970**, *5*, 721–729. [[CrossRef](#)]
41. Klinbumrung, A.; Phuruangrat, A.; Thongtem, T.; Thongtem, S. Synthesis, Characterization and optical properties of BaMoO<sub>4</sub> synthesized by microwave plasma method. *Russ. J. Inorg. Chem.* **2018**, *63*, 725–731. [[CrossRef](#)]
42. Cavalcante, L.S.; Sczancoski, J.C.; Espinosa, J.W.M.; Varela, J.A.; Pizani, P.S.; Longo, E. Photoluminescent behavior of BaWO<sub>4</sub> powders processed in microwave-hydrothermal. *J. Alloys Compd.* **2009**, *474*, 195–200. [[CrossRef](#)]
43. Raghunath, S.; Balan, R. Solvent assisted synthesis and characterization of AMoO<sub>4</sub> (A = Ca, Sr & Ba) nanomaterials. *Mater. Today Proc.* **2021**, *46*, 2930–2933.
44. Benchikhi, M.; Ouatib, R.E.; Guillement-Fritsch, S.; Er-Rakho, L.; Durand, B. Characterization and photoluminescence properties of ultrafine copper molybdate (α-CuMoO<sub>4</sub>) powders via a combustion—Like process. *Int. J. Mener. Metall. Mater.* **2016**, *23*, 13401345. [[CrossRef](#)]
45. Sabri, N.S.; Yahya, A.K.; Talari, M.K. Emission properties of Mn doped ZnO nanoparticles prepared by mechanochemical processing. *J. Lim.* **2012**, *132*, 1735–1739. [[CrossRef](#)]

**Disclaimer/Publisher’s Note:** The statements, opinions and data contained in all publications are solely those of the individual author(s) and contributor(s) and not of MDPI and/or the editor(s). MDPI and/or the editor(s) disclaim responsibility for any injury to people or property resulting from any ideas, methods, instructions or products referred to in the content.